Geomechanics and Engineering, *Vol. 22, No. 4 (2020) 319-328*
DOI: https://doi.org/10.12989/gae.2020.22.4.319

Stability assessment of soil slopes in three dimensions: The effect of the width of failure and of tension crack

Lysandros Pantelidis*[1], Elias Gravanis[1,2a] and Konstantinos-Paraskevas Gkotsis[1b]

[1]*Department of Civil Engineering and Geomatics, Cyprus University of Technology, 2-8 Saripolou str., Limassol 3036, Cyprus*
[2]*Eratosthenes Centre of Excellence, 2-8 Saripolou str., Limassol 3036, Cyprus*

(Received September 10, 2019, Revised July 5, 2020, Accepted July 12, 2020)

Abstract. This paper investigates the effect of the width of failure and tension crack (TC) on the stability of cohesive-frictional soil slopes in three dimensions. Working analytically, the slip surface and the tension crack are considered to have spheroid and cylindrical shape respectively, although the case of tension crack having planar, vertical surface is also discussed; the latter was found to return higher safety factor values. Because at the initiation of a purely rotational slide along a spheroid surface no shear forces develop inside the failure mass, the rigid body concept is conveniently used; in this respect, the validity of the rigid body concept is discussed, whilst it is supported by comparison examples. Stability tables are given for fully drained and fully saturated slopes without TC, with non-filled TC as well as with fully-filled TC. Among the main findings is that, the width of failure corresponding to the minimum safety factor value is not always infinite, but it is affected by the triggering factor for failure (e.g., water acting as pore pressures and/or as hydrostatic force in the TC). More specifically, it was found that, when a slope is near its limit equilibrium and under the influence of a triggering factor, the minimum safety factor value corresponds to a near spherical failure mechanism, even if the triggering factor (e.g., pore-water pressures) acts uniformly along the third dimension. Moreover, it was found that, the effect of tension crack is much greater when the stability of slopes is studied in three dimensions; indeed, safety factor values comparable to the 2D case are obtained.

Keywords: slope stability analysis; analytical solution; tension crack; three-dimensions; triggering factor for failure

1. Introduction

During the last decades a great number of 3D slope stability analysis methods has been proposed, either limit equilibrium (Anagnosti 1969, Chen and Chameau 1983, Chen *et al.* 2003, Cheng and Yip 2007, Gens *et al.* 1988, Hovland 1979 Huang *et al.* 2002, Hungr 1987, Hungr *et al.* 1989, Leshchinsky *et al.* 1985, Leshchinsky and Huang 1992, Sun *et al.* 2012, Ugai 1988, Xing 1988, Yamagami and Jiang 1997, Zhou and Cheng 2013) or limit analysis ones (Ganjian *et al.* 2010, Gao *et al.* 2013, Michalowski 2010 Michalowski and Drescher 2009, Michalowski and Tabetha 2011, Nadukuru *et al.* 2011, Pan *et al.* 2017). In addition, Liu *et al.* (2017) proposed a three-dimensional slope stability analysis method using independent cover based numerical manifold and vector method, whilst Yamaguchi *et al.* (2018) a three-dimensional simplified slope stability analysis based on the hybrid-type penalty method. Zhang *et al.* (2013b) studied the effects of complex geometries on three-dimensional (3D) slope stability using an elastoplastic finite difference method (FDM) with a strength reduction technique, Jeldes *et al.* (2015) offered an approximate solution to the Sokolovskiĭ concave slope at limiting equilibrium, whilst Zhang *et al.* (2013a) proposed an analytical method to evaluate the effect of a turning corner on 3D slope stability. Zhang *et al.* (2017), in turn, offered a 3D stability analysis method of concave slope based on the Bishop method. Yang and Xu (2017) investigated the influence of strength inhomogeneity on the seismic and static 3D stability of a two-stage slope based on limit analysis. Xu *et al.* (2018), Gao *et al.* (2014), Lim *et al.* (2016) and Sun *et al.* (2017) offered 3D slope stability charts for nonhomogeneous and anisotropic soils, four different types of drawdown processes, frictional fill materials over purely cohesive clay and convex and concave slopes in plan-view consisting of homogeneous soil respectively. Sun *et al.* (2019) used a modified strength reduction finite element method to propose stability charts for pseudostatic stability analysis of three-dimensional (3D) homogeneous soil slopes subjected to seismic excitation. Xu and Yang (2018) offered three-dimensional stability analysis of slope in unsaturated soils considering strength nonlinearity under water drawdown. Furthermore, Gao *et al.* (2016) suggested a 3D rock slope stability limit analysis method using non-linear failure criterion, while Yang (2017) studied the effect of pore-water pressure on 3D stability of rock slopes. Lin *et al.* (2020) investigated the effect of the dilatancy angle on slope stability using the 3D finite element method strength reduction technique. Review of the various three-dimensional limit equilibrium slope stability methods is out of the scope of the present paper; besides, the vast majority of the above mentioned works have already been reviewed by Kalatehjari and Ali (2013)

*Corresponding author, Assistant Professor
E-mail: Lysandros.pantelidis@cut.ac.cy
[a]Ph.D.
[b]M.Sc.

http://www.techno-press.org/?journal=gae&subpage=7
ISSN: 2005-307X (Print), 2092-6219 (Online)

and Chakraborty and Goswami (2016).

Application of the various 3D slope stability methods (e.g., Chen and Chameau 1983, Morimasa and Miura 2008, Michalowski and Drescher 2009), generally, refer to fully drained slopes without the influence of tension crack and indicates that a 3D analysis is always less conservative compared to the respective 2D analysis. Very recently, Wang *et al.* (2019) studied the influence of tension crack in the stability of slopes in three-dimensions. More specifically, they developed an upper bound limit analysis solution to evaluate the 3D stability of unsaturated soil slopes with tension crack under steady infiltration conditions. They concluded that, the effect of crack on slope stability generally decreases with reducing the inclination angle and increases with increasing the width constraint B/H (B and H are the width of the landslide measured on the slope face and the slope height respectively). The stability of slopes can also be evaluated with the finite element (FE) method. However, the later has the major disadvantage that the FE mesh cannot break to form crack were tension exists. As known, depending on the case, the safety factor of a slope in a 2D analysis can be by 20% lower when the effect of tension crack is considered (see Baker 1981); this statement has been validated by the first author working with the 2D closed-form solution proposed by Pantelidis and Griffiths (2013b).

In the present paper, the effect of the third dimension and tension crack (TC) on the stability of soil slopes is investigated. The analysis is based on the 3D analytical solution for the stability analysis of homogenous, cohesive-frictional slopes proposed by Pantelidis and Griffiths (2013a). Working with infinite number of vertical columns and their associated vertical and horizontal intercolumn forces, Pantelidis and Griffiths offered a solution for slides along spherical surfaces (see appendix in Pantelidis and Griffiths 2013a; for the 2D case, that is, for sliding along a circular arc or cylindrical surface of infinity length, see Pantelidis and Griffiths 2013b). The same authors have also shown that the resultant gravity force of the sliding mass (assumption of rigid body), when projected onto the (spherical) failure surface and split into two components (one tangential and one radial), returns the same safety factor value with the rigorous analysis based on infinite number of columns mentioned above. A comparison graph between the 2D analytical solution proposed by Pantelidis and Griffiths (2013b) and Bishop's (1955) method of slices for various water table levels inside the slope mass is given in the next section. As it will be shown, the two methods give similar results. Regarding the three-dimensions, for the example slope with $c'/\gamma H$ = 0.116, φ'=15° and inclination angle 60° presented by Leshchinsky *et al.* (1985), the latter reported a safety factor value F = 1.25, Hungr *et al.* (1989) F = 1.230 with their 3D simplified Bishop method, Huang *et al.* (2002) F = 1.204 and 1.243 with their simplified and rigorous limit equilibrium method respectively and Pantelidis and Griffiths (2013a) F = 1.258 considering spherical failure surface. All these safety factor values refer to fully drained slopes, whilst the possible development of tension crack has been ignored. As in the case of circular and spherical failure surfaces, because at the initiation of a purely rotational slide along a spheroid surface no shear forces are developed inside the failure mass, the rigid body concept is valid and thus, it is conveniently used in the analysis below in studying the effect of the third dimension and tension crack on the stability of soil slopes.

2. Methodology

The preliminary analysis carried out by the authors showed that a tension crack of vertical, cylindrical shape produces lower safety factor values comparing to a tension crack of vertical, planar surface. An example case comparing the two cases is illustrated in Fig. 1. Thus, hereafter, the tension crack is simulated by the curved surface of a cylinder having axis of rotation parallel to the y-axis; the problem is considered symmetrical as for the xy-plane and, thus, the axis of rotation of the cylinder intersects the x-axis. The rational assumption that the periphery of the cylinder passes through the points intersecting the failure surface, the slope face and the slope crest (points M and N in Fig. 1; left case) has also been made. The failure surface is considered to be of spheroid shape defined by the radius r, which is the rotation arm measured from the centre of rotation to the failure surface on the plane of symmetry and the radius R defining the half width of the spheroid (the ratio of the two radii defines the parameter f; $f = R/r$). The f = 1 case is presented in Fig. 1 for illustration purposes.

Adopting Coulomb's failure criterion, the safety factor for the simple geometry shown in Fig. 1 (left) and Fig. 2 considering only the self-weight of the sliding mass and the effect of pore water pressures, is given by the following equation:

$$F = \frac{c'A + (W\cos\delta_1 - U)\tan\varphi'}{W\sin\delta_1}$$
$$\text{or} \tag{1}$$
$$F = \frac{rc'A + r(W\cos\delta_1 - U)\tan\varphi'}{rW\sin\delta_1}$$

where, c' and φ' are the effective shear strength parameters of soil, A is the surface area of the sliding mass, W and U are the resultant weighing force of the sliding mass and the resultant hydrostatic force acting radially on the slip surface respectively and $\delta_1 = \pi/2 - \delta$; see Fig. 2. An iterative (optimization) procedure is needed for obtaining the minimum safety factor value; the optimization parameters are five, namely, the coordinates of the center of rotation (x_o, y_o), the two radii of the spheroid (r and R) and the x-coordinate of the axis of cylinder (x_{cyl}). However, for studying the effect of the third dimension on the stability of slopes and, simultaneously, reducing the CPU time, the radius R in the parametric analysis of the next sections is manually changed.

For calculating the resistance to sliding due to cohesion, the area of slip surface is needed (recall Eq. (1)). This is calculated exactly as follows (see Arfken *et al.* 2012):

$$A = 2\begin{pmatrix} \int_{x_{cyl}-R_{cyl}}^{H/\tan\beta}\int_0^{z_{in}} s(x,z)dzdx + \\ +\int_{H/\tan\beta}^{0}\int_0^{z_{out}} s(x,z)\,dzdx \end{pmatrix} \tag{2}$$

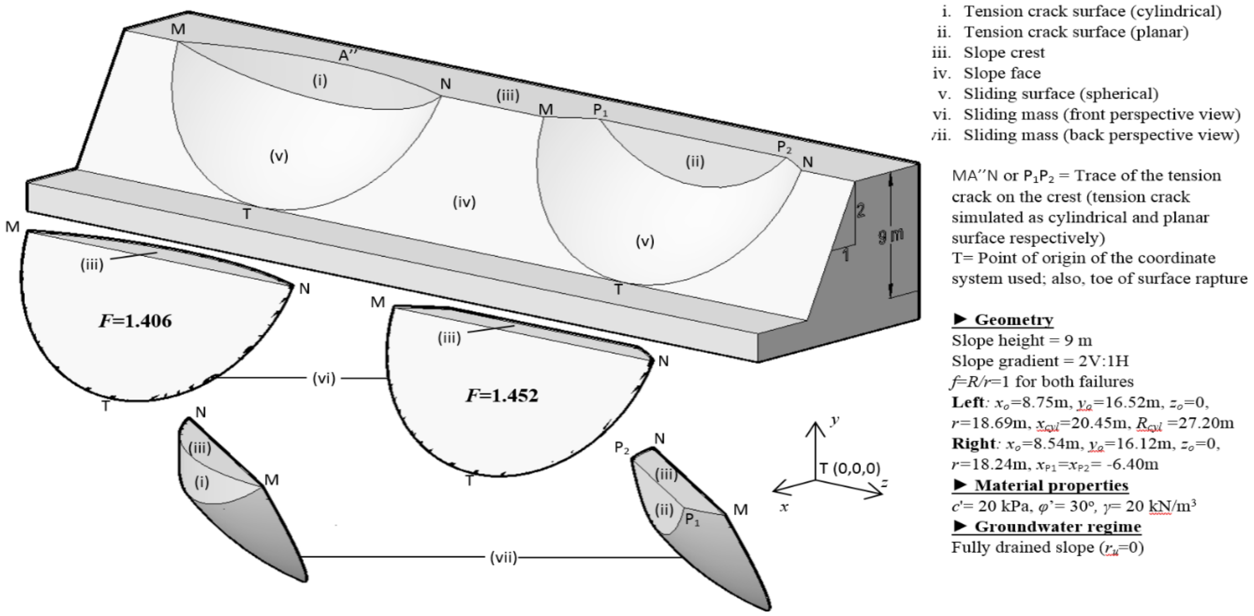

Fig. 1 Perspective view of the failure surface and the sliding mass of an example slope for the case of tension crack of cylindrical and planar shape (left and right set of drawings respectively). Optimization for finding the minimum safety factor value in both cases was involved

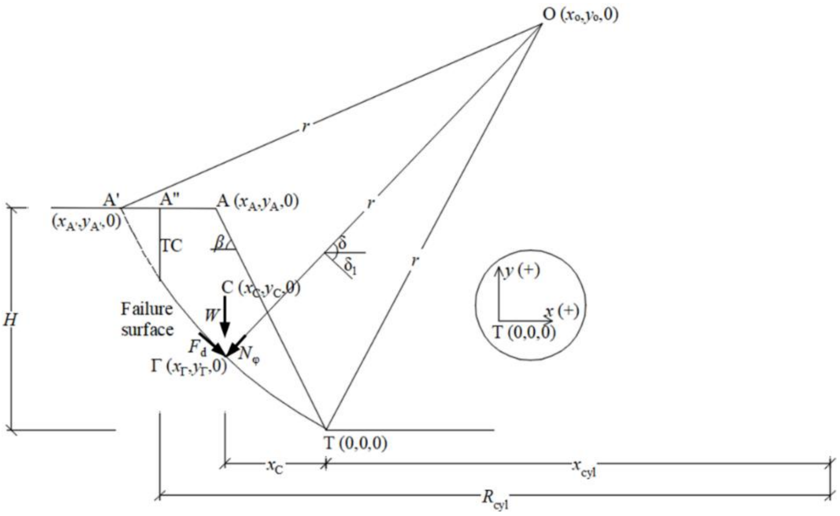

Fig. 2 Definition of symbols used in the analysis. Case of tension crack of cylindrical shape. Figure showing the cross-section for $z = 0$ (plane of symmetry, xy)

with

$$s(x,z)=\sqrt{1+\left(\frac{d\{y_s(x,z)\}}{dx}\right)^2+\left(\frac{d\{y_s(x,z)\}}{dz}\right)^2} \tag{3}$$

where, the function $y_s(x,z)$ is obtained solving the equation of spheroid as for the y-coordinate:

$$y_s(x,z)=y_o-\sqrt{\left(1-\frac{z^2}{R^2}\right)r^2+(x-x_o)^2} \tag{4}$$

The z_{in} integral limit is defined by the equation of cylinder

$$z_{in}=\sqrt{R_{cyl}^2-(x-x_{cyl})^2} \tag{5}$$

whilst the z_{out} limit by the intersection between the spheroid and the slope face (curve MTN in Fig. 2)

$$z_{out}=R\sqrt{1-\frac{(x\tan\beta-y_o)^2+(x-x_o)^2}{r^2}} \tag{6}$$

W is calculated as follows,

$$W=2\gamma\left(\begin{array}{l}\int_{x_{cyl}-R_{cyl}}^{H/\tan\beta}\int_0^{z_{in}}\left[H-y_s(x,z)\right]dzdx+\\ \int_{H/\tan\beta}^{0}\int_0^{z_{out}}\left[x\tan\beta-y_s(x,z)\right]dzdx\end{array}\right) \tag{7}$$

Also, from Fig. 2

$$\delta=\arctan\frac{y_\Gamma-y_o}{x_C-x_o} \tag{8}$$

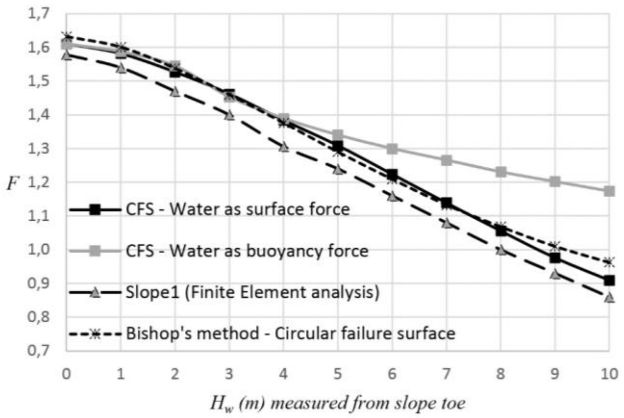

Fig. 3 Comparison example for investigating the action of water in slope stability analysis; the notation "CFS" refers to the closed-form solution proposed by Pantelidis and Griffiths (2013b)

where, the x-coordinate of the center of the sliding mass, x_C, is

$$x_C = \frac{2\gamma}{W}\left(\begin{array}{l} \int_{x_{cyl}-R_{cyl}}^{H/\tan\beta} \int_0^{z_{in}} x\left[H - y_s(x,z)\right] dzdx + \\ \int_{H/\tan\beta}^{0} \int_0^{z_{out}} x\left[x\tan\beta - y_s(x,z)\right] dzdx \end{array} \right) \quad (9)$$

and the y-coordinate of the point where the vector of W is projected on the spheroid surface is

$$y_\Gamma = y_o - \sqrt{r^2 - (x_C - x_o)^2} \quad (10)$$

Generally, the water in slope mass can be treated as either buoyancy or surface force; please compare Eq. (C-12) with (C-13) in EM 1110 (US Army Corps of Engineers, 1990). Working with the 2D version of the closed-form solution (CFS) of Pantelidis and Griffiths (2013b), the authors found that considering water as surface force, the method returns absolutely comparable safety factor values with those obtained using the Finite Element method* or the Limit Equilibrium method; such a comparison in given in Fig. 3 (slope referring to c' = 20 kPa, φ' = 31°, γ = 20 kN/m^3, $\tan\beta$ = 1 and H = 10 m; H_w is the height of the water table which is considered horizontal and does not extend outside the slope; H_w is measured from slope toe). Thus, water herein is treated as surface force.

Assuming that the water table is horizontal inside the soil mass and that, it cannot exceed in height the geometry of slope, U is calculated as follows,

$$U = 2\gamma_w \left(\begin{array}{l} \int_{x_{cyl}-R_{cyl}}^{H_w/\tan\beta} \int_0^{z_{in}} \left[H_w - y_s(x,z)\right] s(x,z)\, dzdx + \\ +\int_{H_w/\tan\beta}^{0} \int_0^{z_{out}} \left[x\tan\beta - y_s(x,z)\right] s(x,z)\, dzdx \end{array} \right) \quad (11)$$

Finally, the safety factor is calculated using Eq. (1). It is reminded that the effect of water-filled tension crack has not yet been considered. As known, the additional hydrostatic force due to water in the tension crack lowers the safety factor. In this respect, the moment of the resultant hydrostatic force V due to the water in the tension crack is added in the denominator of the safety factor equation:

$$F = \frac{rc'A + r(W\cos\delta_1 - U)\tan\varphi'}{rW\sin\delta_1 + V(y_o - y_w)} = \frac{c'A + (W\cos\delta_1 - U)\tan\varphi'}{W\sin\delta_1 + \frac{(y_o - y_w)}{r}V} \quad (12)$$

One could subtract this moment from the numerator, taking:

$$F = \frac{c'A + (W\cos\delta_1 - U)\tan\varphi' - \frac{(y_o - y_w)}{r}V}{W\sin\delta_1} \quad (13)$$

However, the latter is not consistent with the definition of safety factor with respect to shear strength of soil. Instead, other factoring strategies could be explored, such as, the one with respect to U (see also Pantelidis and Griffiths 2012, 2013c):

$$\begin{array}{l} c'A + (W\cos\delta_1 - U\cdot F)\tan\varphi' = W\sin\delta_1 + \frac{y_o - y_w}{r}V \Rightarrow \\ F = \frac{W\cos\delta_1 - \left(W\sin\delta_1 + \frac{y_o - y_w}{r}V - c'A\right)\frac{1}{\tan\varphi'}}{U} = \frac{U_{\lim}}{U} \end{array} \quad (14)$$

where, U_{lim} is the hydrostatic force corresponding to a just stable slope and U is the available hydrostatic force. However, this is beyond the scopes of the present paper.

Eq. (12) needs both V and y_w to be known. These magnitudes can be calculated as follows:

$$V = 2\int_{y_s\left(x_{cyl} - \sqrt{R_{cyl}^2 - z^2}\right)}^{y_{wtc}} \int_0^{z_{Mw}} \left[\gamma_w (y_{wtc} - y)\cos\left(\arcsin\frac{z}{R_{cyl}}\right)\right] dzdy \quad (15)$$

$$y_w = \frac{1}{V}\int_{y_s\left(x_{cyl} - \sqrt{R_{cyl}^2 - z^2}\right)}^{y_{wtc}} \int_{-z_{Mw}}^{z_{Mw}} \left[\begin{array}{l} \gamma_w (y_{wtc} - y)\cdot \\ \cos\left(\arcsin\frac{z}{R_{cyl}}\right) y \end{array}\right] dzdy \quad (16)$$

where, from the equation of cylinder for $x = x_{Mw}$

$$z_{Mw} = \sqrt{R_{cyl}^2 - (x_{Mw} - x_{cyl})^2} \quad (17)$$

with x_{Mw} to be obtained from $y = y_{wtc}$ and the equations of spheroid and cylinder, i.e.,

$$x_{Mw} = \frac{R^2 x_o - r^2 x_{cyl} + \sqrt{\begin{array}{l} r^4\left(R_{cyl}^2 - R^2\right) - R^4\left(y_o - y_{wtc}\right)^2 + \\ +(rR)^2\left(\begin{array}{l} R^2 - R_{cyl}^2 + \\ \left(x_o - x_{cyl}\right)^2 + \\ \left(y_o - y_{wtc}\right)^2 \end{array}\right) \end{array}}}{(R-r)(R+r)} \quad (18)$$

The hydrostatic water pressure $\gamma_w(y_{wtc}-y)$ in Eq. (15)

*The freely available finite element program Slope1 for slope stability analysis was used http://inside.mines.edu/fs_home/vgriffit/

(also in Eq. (16)) is multiplied by a cosine term because only the component parallel to the direction of sliding (i.e., along the x-axis) contributes to failure. In this respect, the z-components cancel-out due to the symmetry of the problem.

3. Results

Stability tables are given for the following six cases: (1) Fully drained slopes without TC (Table 1), (2) Fully saturated slopes without TC (Table 2), (3) Fully drained slopes with non-filled TC (Table 3), (4) Fully drained slopes with fully-filled TC (Table 4), (5) Fully saturated slopes with non-filled TC (Table 5) and (6) Fully saturated slopes with fully-filled TC (Table 6) both for R/r = 1 and 2. The stability factor, N_F, or the stability number (m=1/N_F) concept provides the basis for the development of stability charts or tables (e.g., Taylor 1948, Spencer 1967, Janbu 1954, 1967, 1968, Cousins 1978, 1980, Pantelidis and Psaltou 2012). The stability factor N_F is given as follows:

$$N_F = \gamma H F / c' \tag{19}$$

The dimensionless parameter $\lambda_{c\varphi}$ (introduced by Spencer 1967) is given by the following ratio

$$\lambda_{c\varphi} = \gamma H \tan\varphi' / c' \tag{20}$$

and it also groups terms related to the slope stability problem. The safety factor is finally calculated using the following equation:

$$F = N_F\, c'/\gamma H = \left(N_F / \lambda_{c\varphi}\right) \tan\varphi' = \Lambda \tan\varphi' \tag{21}$$

where, $\Lambda = N_F/\lambda_{c\varphi}$. Λ values are given in tabular form in Tables 1 to 6 for the six cases mentioned previously; the following $\lambda_{c\varphi}$ values were considered: $\lambda_{c\varphi}$ = 1, 2, 5, 10, 20 and 50.

For cases between a fully drained and a fully saturated slope, the r_u concept can be used; Bishop and Morgenstern (1960) have shown that for a given slope, the relationship between F and r_u does not differ appreciably from the straight line. Thus, between a fully drained (r_u = 0) and a fully saturated slope ($r_u = \gamma_w/\gamma$; see Pantelidis and Psaltou 2012), linear interpolation can be applied. Eq. (12) in r_u-form is:

$$F = \frac{c' A + W \cos\delta_1 \left(1 - r_u\right) \tan\varphi'}{W \sin\delta_1 + \dfrac{\left(y_o - y_w\right)}{r} V} \tag{22}$$

where, the r_u ratio corresponding to the overall sliding mass is $U/W\cos\delta_1$.

An important observation is that, if in each trial solution in finding the most critical slip surface, the tension crack is considered to be a priory fully-filled with water, the minimum F always correspond to $R_{cyl} \rightarrow \infty$. That is, the tension crack tends to be a vertical, planar surface passing through the points M and N (see Fig. 2). Obviously, this is not the point in practice. When a tension crack forms, it is not instantaneously filled with water, even if the slope is fully saturated; on the other hand, if a tension crack has not yet formed, any relevant hydrostatic force does not exist. As

Table 1 Λ values for Case 1 (fully drained slopes without TC)

R/r	tanβ	$\lambda_{c\varphi}$					
		1	2	5	10	20	50
1	1:2	12.162	7.727	4.851	3.773	3.304	2.644
	1:1.5	11.311	7.024	4.327	3.166	2.622	2.070
	1:1	10.413	6.211	3.622	2.478	1.976	1.475
	2:1	8.663	5.003	2.695	1.839	1.342	0.965
	4:1	7.397	4.237	2.242	1.497	1.058	0.718
	8:1	6.693	3.806	2.008	1.314	0.912	0.595
2	1:2	11.583	7.583	4.773	3.720	3.267	2.635
	1:1.5	10.790	6.721	4.239	3.116	2.593	1.997
	1:1	9.813	5.965	3.510	2.445	1.887	1.470
	2:1	8.327	4.837	2.637	1.815	1.328	0.969
	4:1	7.191	4.147	2.213	1.484	1.052	0.715
	8:1	6.578	3.762	1.985	1.313	0.911	0.594

Table 2 Λ values for Case 2 (fully saturated slopes without TC)

R/r	tanβ	$\lambda_{c\varphi}$					
		1	2	5	10	20	50
1	1:2	9.726	5.695	3.029	2.038	1.504	1.209
	1:1.5	9.292	5.255	2.618	1.666	1.166	0.829
	1:1	8.745	4.746	2.212	1.246	0.716	0.364
	2:1	7.512	3.866	1.567	0.643		
	4:1	6.341	3.183	1.121			
2	1:2	9.403	5.462	3.001	2.049	1.543	1.249
	1:1.5	8.735	5.021	2.579	1.721	1.211	0.857
	1:1	8.202	4.510	2.137	1.240	0.735	0.394
	2:1	7.192	3.703	1.527	0.634		
	4:1	6.121	3.090	1.084			

Table 3 Λ values for Case 3 (fully drained slopes with non-filled TC)

R/r	tanβ	$\lambda_{c\varphi}$					
		1	2	5	10	20	50
1	1:2	11.997	7.716	4.821	3.662	3.097	2.581
	1:1.5	10.917	6.829	4.150	3.121	2.516	2.063
	1:1	9.765	6.021	3.453	2.405	1.925	1.474
	2:1	7.527	4.555	2.488	1.738	1.293	0.947
	4:1	5.876	3.553	1.951	1.350	0.983	0.687
	8:1	4.878	2.920	1.629	1.117	0.804	0.552
2	1:2	11.352	7.384	4.655	3.614	3.065	2.581
	1:1.5	10.377	6.576	4.040	3.091	2.507	1.995
	1:1	9.160	5.619	3.278	2.387	1.860	1.468
	2:1	7.210	4.352	2.437	1.714	1.281	0.943
	4:1	5.794	3.452	1.934	1.340	0.979	0.685
	8:1	4.867	2.914	1.621	1.116	0.803	0.551

Table 4 Λ values for Case 4 (fully drained slopes with fully-filled TC)

R/r	$\tan\beta$	$\lambda_{c\varphi}$					
		1	2	5	10	20	50
1	1:2	11.850	7.585	4.816	3.650	3.062	2.539
	1:1.5	10.749	6.763	4.059	3.090	2.508	2.025
	1:1	9.471	5.688	3.401	2.387	1.859	1.471
	2:1	6.821	4.087	2.339	1.664	1.247	0.933
	4:1	4.578	2.804	1.672	1.204	0.910	0.656
	8:1	3.355	2.163	1.229	0.879	0.676	0.503
2	1:2	11.225	7.316	4.630	3.604	3.002	2.539
	1:1.5	10.189	6.487	3.967	3.085	2.500	1.863
	1:1	8.876	5.472	3.268	2.362	1.850	1.464
	2:1	6.594	4.018	2.285	1.643	1.243	0.931
	4:1	4.827	2.930	1.716	1.208	0.914	0.658
	8:1	3.384	2.174	1.268	0.891	0.681	0.506

Table 5 Λ values for Case 5 (fully saturated slopes with non-filled TC)

R/r	$\tan\beta$	$\lambda_{c\varphi}$					
		1	2	5	10	20	50
1	1:2	9.470	5.565	2.984	2.018	1.502	1.157
	1:1.5	9.006	5.064	2.555	1.641	1.164	0.786
	1:1	8.161	4.446	2.171	1.215	0.705	0.362
	2:1	6.374	3.331	1.372	0.564		
	4:1	4.890	2.481	0.821			
2	1:2	8.979	5.329	2.959	2.035	1.534	1.183
	1:1.5	8.355	4.800	2.512	1.706	1.190	0.808
	1:1	7.645	4.204	2.037	1.201	0.733	0.379
	2:1	6.099	3.202	1.337	0.587		
	4:1	4.742	2.405	0.803			

Table 6 Λ values for Case 6 (fully saturated slopes with fully-filled TC)

R/r	$\tan\beta$	$\lambda_{c\varphi}$					
		1	2	5	10	20	50
1	1:2	9.358	5.508	2.968	2.013	1.500	1.156
	1:1.5	8.870	4.994	2.535	1.635	1.162	0.786
	1:1	7.923	4.332	2.037	1.151	0.714	0.362
	2:1	5.791	3.095	1.312	0.559		
	4:1	4.045	2.125	0.783			
2	1:2	8.814	5.274	2.942	2.030	1.533	1.183
	1:1.5	8.165	4.733	2.494	1.698	1.188	0.808
	1:1	7.384	4.100	2.017	1.193	0.726	0.378
	2:1	5.737	2.918	1.274	0.577		
	4:1	4.038	2.116	0.764			

known, tension crack develops as part of the initial phase of failure, where stress redistribution takes place in slope; slope failure may follow or not. At a later phase, if failure has not occurred, the tension crack can be (fully or partially) filled with water (either surface water, rainwater falling directly in the TC or water drained from the soil mass), deteriorating the stability condition of slope. Given that tension crack develops in cohesive soils having very low to extremely low permeability, these thoughts can be considered rational. Thus, in this paper, when the hydrostatic force due to water in tension crack is considered, the analysis is based on the idea that, first the tension crack develops and later this is filled with water; the most unfavourable case of fully-filled tension crack is examined.

4. Discussion

4.1 The role of the third dimension on the stability of soil slopes

Before discussing on the role of the third dimension on the stability of slopes, it is important to be reminded that, water, either in the slope mass (forming free water table) or in the tension crack (exerting hydrostatic pressure), could potentially trigger the failure of a slope. Moreover, it is mentioned that, although the presence of tension crack lowers the safety factor of slope, the tension crack alone is not a triggering factor for failure.

Comparing, now, the Λ values given in Tables 1 to 6 for the six cases numbered in the previous section, the following major observations can be made.

When there is no water in the slope or in the tension crack, the Λ values for $R/r = 1$ are always greater than the respective ones for $R/r = 2$ (see Tables 1 and 3). Actually, the F - R/r relationship follows a reciprocal function of the form

$$F = F_{R/r\to\infty} + \frac{a}{R/r - \left(R/r\right)_{\min}} \tag{23}$$

where, $F_{R/r\to\infty}$ is the minimum safety factor value (asymptotic value corresponding to $R/r\to\infty$) and α is a coefficient (natural positive number). Also, there is a minimum allowable R/r value, $(R/r)_{\min}$; when R/r tends to this value, F becomes asymptotically infinite.

The same behaviour is also observed for fully saturated slopes with strong slope gradient and small $\lambda_{c\varphi}$ value. However, for fully saturated slopes with small slope gradient and great $\lambda_{c\varphi}$ value, the $R/r = 2$ case was found to be less conservative compared to the $R/r = 1$ case (see Tables 2, 5 and 6). This characteristic behaviour is illustrated in Fig. 4. The presence of tension crack, filled or not with water, does not cause any qualitative difference.

Finally, for drained slopes but with fully-filled tension crack, the $R/r = 2$ case was found to be more conservative as compared to the $R/r = 1$ case for great slope gradients (see Table 4). However, for gentle slope gradients, the opposite stands.

Apparently, for any intermediate case between a fully drained and a fully saturated slope, either the $R/r = 1$ or the $R/r = 2$ case is unfavorable depending on the height of the

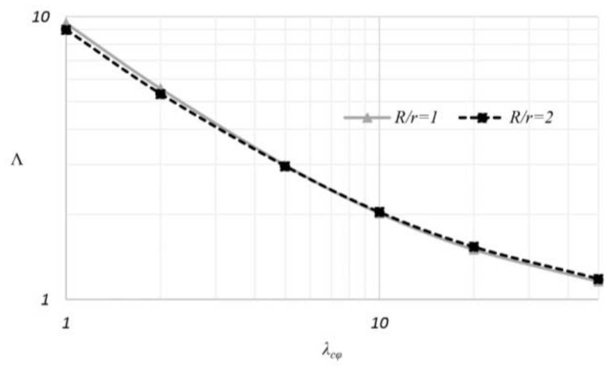

Fig. 4 $\lambda_{c\varphi}$ versus Λ example chart for fully saturated slope with $\tan\beta$ = 1:2 and no water in TC; curves referring to R/r = 1 and 2

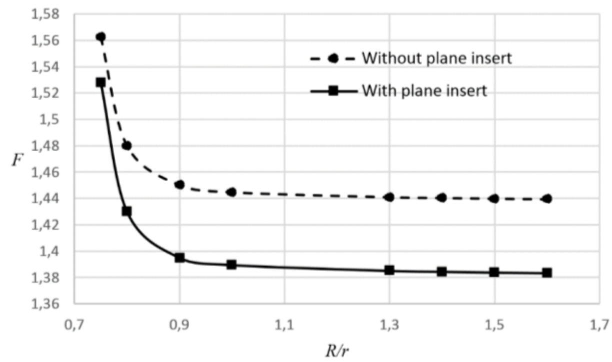

Fig. 5 R/r versus F example chart for fully drained slopes, with and without plane insert

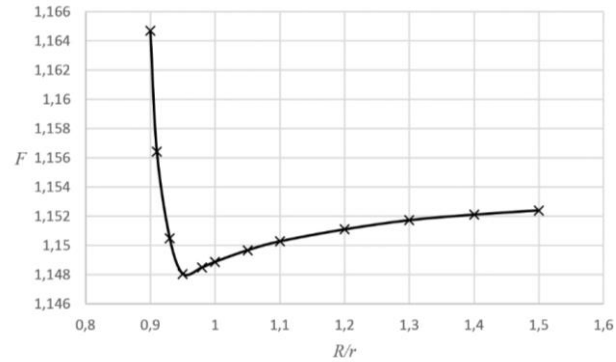

Fig. 6 R/r versus F example chart for fully saturated slope (no plane insert)

water table in the slope and the stability level of the latter (deviation from its limit equilibrium). An analogous conclusion can be drawn for partially filled tension cracks.

This characteristic behaviour, where, a wider failure surface may be more favourable than a respective narrower for the same slope, is further discussed later.

4.2 The end-effect of landslides

Morimasa and Miura (2008) studied analytically the end-effect of landslides in purely cohesive slopes considering spheroid failure surfaces. They provided N_F – w_{sld}/H charts for completely drained slopes with inclination angle ranging from 15° to 90° (w_{sld} is the half width of the landslide). In all their cases, the stability factor N_F is reduced exponentially following a reciprocal function form (recall Eq. (23)).

In their 3D analysis, Chen and Chameau (1983), Michalowski and Drescher (2009) and Michalowski (2010), studied the stability of slopes with a plane insert (extruded to the third dimension) in the central portion of the failure mechanism. The latter assures that the combined mechanism tends (asymptotically) to a plane strain mechanism when no constraints are placed on the mechanism width; the geometry of this insert is identical to the geometry of the plane mechanism considered by Chen *et al.* (1969). Michalowski (2010) additionally observed that a footing of finite dimensions in plan-view on the crest of a 3D slope restrains the width of failure from becoming infinite. However, a surcharge on the crest of slope is a local triggering factor, and therefore, a local failure is, logically, expected. Contrary to this, the authors have shown through Tables 1-6 and Fig. 4 that, depending on the case, a narrower slope failure may by more critical, even if pore pressures are uniformly distributed along the third dimension.

The above, non-usual, behaviour led to a more thorough investigation of the end-effect of landslide. First, it is mentioned that, the double asymptotic behaviour (F taking its minimum value for infinite failure width and F becoming infinite for a given failure width value; recall Eq. (23)) is, generally, confirmed by the authors. In this respect, two example curves are given in Fig. 5, with and without the so-called "plane insert"; the total width of the cylindrical part added at the central portion of the failure mass was equal to one slope height. The slope had the following soil, geometric and groundwater regime properties: c' = 20 kPa, φ' = 30°, γ = 20 kN/m^3, $\tan\beta$ = 2, H = 9 m and r_u = 0 (fully drained slope). It is interesting that the plane insert does not affect the minimum allowable landslide width (see Fig. 5). It is more interesting, however, that, as shown in the proposed tables, the R/r = 1 case may give smaller safety factor value than the R/r = 2 case for the same slope. In this respect, a F - R/r example curve is given in Fig. 6 for a fully saturated slope having c' = 14 kPa, φ' = 35°, γ = 20 kN/m^3, $\tan\beta$ = 2/3 and H = 10 m. The curve in question also presents two asymptotic branches, however, the right branch approaches an asymptotic F value (F≈1.153) from below, after reaching first a minimum value (F≈1.148). Indeed, the minimum F value corresponds to a nearly spherical failure surface (R/r = 0.95). This clearly indicates that, when the z-coordinate (it refers to the third axis defining the 3D geometry) of the centre of rotation in a three-dimensional slope stability analysis is fixed and the slope has uniform properties along its length (similar to plane strain conditions), the minimum safety factor does not always correspond to a failure mechanism of infinite width; instead a spherical or nearly spherical failure may occur. Apparently, in practice, local changes in slope geometry or material properties affects not only the safety factor of slope but also the location of the z-coordinate of the centre of rotation.

It is additionally noted that, the safety factor value against circular failure (analysis in two dimensions) of the above-mentioned slope using Bishop's (1955) limit equilibrium method with Rocscience's SLIDE, was found equal to 1.102. This value is by only 4% lower compared to the minimum F value given in Fig. 6 (F = 1.148 for R/r = 0.95). Regarding the depth of tension crack, the analysis with (2D) Bishop's method of slices gave 1.2 m, whilst, the maximum depth (on the plane of symmetry) using the present analytical procedure was 1.83 m.

4.3 The effect of tension crack on the safety factor of slopes

The presence of tension crack in slopes indicates that, in a certain zone the tensile stresses exceed the tensile strength of the medium. The tension crack affects the stability of slope mainly because it reduces the area of the slip surface (thus, reducing the resistance to failure) and because the water pressure acting on the crack face constitutes an additional driving force contributing to failure (Baker, 1981). Baker (1981) found that the (maximum) decrease in the stability factor (N_F) due to the presence of non-filled tension crack is of the order of 20%. He also found that, the maximum depth of the tension crack is 25% of the slope height; the latter corresponds to vertical slopes.

Based on the slope cases considered herein (i.e., $\lambda_{c\varphi}$ ranging from 1 to 10 and tanβ ranging from 1:2 to 8:1), the maximum relative difference in Λ, i.e., $(\Lambda_{max} - \Lambda_{min})/\Lambda_{max}$, due to the presence of tension crack was found to be of the order of 27% for non-filled cracks and 50% for fully-filled cracks; numbers referring to fully drained slopes. For fully saturated slopes, the maximum relative difference in Λ is of the order of 25% and 35% for non-filled and fully-filled tension cracks respectively. [Defining the relative difference with respect to the minimum Λ value, i.e., $(\Lambda_{max} - \Lambda_{min})/\Lambda_{min}$, the above-mentioned relative difference values are much higher].

4.4 The effect of water level in tension crack on the stability of soil slopes

The effect of water level in tension crack on the stability of soil slopes is shown schematically in the example chart of Fig. 7. This Λ versus 'percentage of tension crack height (at z = 0 m) filled with water' chart refers to the case of a fully drained slope with $\lambda_{c\varphi}$ = 1 and 8V:1H gradient. From the figure in question it is inferred that, the driving force due to water in tension crack has negligible effect on the stability of slopes when the tension crack is filled with water up to about the one third of its maximum depth (measured from the lowest point); the effect becomes more significant as the water level rises in the tension crack. Wang *et al.* (2019) draw a similar conclusion based on limit analysis. In addition, comparing Table 3 with Table 4 or Table 5 with Table 6 it is concluded that, the effect of water in tension crack on the stability is negligible in gentle slopes (regardless of the $\lambda_{c\varphi}$ ratio) and significant in steeper slopes with small $\lambda_{c\varphi}$ values.

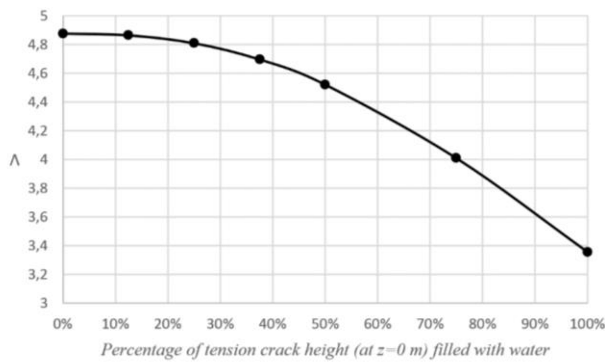

Fig. 7 Example chart showing the effect of water height in tension crack on slope stability

5. Conclusions

In this paper, the effect of the third dimension and tension crack (TC) on the stability of soil slopes is investigated. The analysis is based on the 3D closed-form solution for homogenous, cohesive-frictional slopes proposed by Pantelidis and Griffiths (2013a). Pantelidis and Griffiths' (2013a) method has been extended herein as to consider purely rotational slides along spheroid surfaces as well as the development of tension crack in the slope. Stability tables are given for fully drained and fully saturated slopes without TC, with non-filled TC as well as with fully-filled TC.

Among the main findings is that, the width of failure is related to the triggering factor for failure, in this respect, water acting as pore pressures and/or as hydrostatic force in the TC. More specifically, it was found that, when a slope is near its limit equilibrium and under the influence of a triggering factor, the failure mechanism is restricted to a certain width, even if the triggering factor (e.g., pore-water pressures) is uniformly distributed along the third dimension. Indeed, a spherical or nearly spherical failure surface is more probable to occur than an oblate or prolate failure surface. This contrasts with the current knowledge that, the minimum safety factor of a slope in a 3D analysis corresponds always to infinite failure width.

Moreover, it was found that, the effect of tension crack is much greater when the stability of slopes is studied in three dimensions. Indeed, the safety factor derived from a 3D analysis considering the effect of tension crack is comparable to the respective one derived from a 2D analysis. Finally, it is mentioned that the effect of hydrostatic force due to water in tension crack on the stability of slopes is negligible when the height of water in tension crack does not exceed about the one third of its (maximum) depth but becomes significant as water rises in it.

References

Anagnosti, P. (1969), "Three dimensional stability of fill dams", *Proceeding of 7th International Conference on Soil Mechanics and Foundation Engineering*, Mexico City, Mexico, August.

Arfken, G.B., Weber, H.J. and Harris, F.E. (2012), *Mathematical methods for physicists*, Academic, Elsevier, New York, U.S.A.

Baker, R. (1981), "Tensile strength, tension cracks and stability of slopes", *Soils Found*., **21**(2), 1-17. https://doi.org/10.3208/sandf1972.21.2_1.

Bishop, A.W. (1955), "The use of the slip circle in the stability analysis of slopes", *Géotechnique*, **5**(1), 7-17. https://doi.org/10.1680/geot.1955.5.1.7.

Bishop, A.W. and Morgenstern, N. (1960), "Stability coefficients for earth slopes", *Géotechnique*, **10**(4), 129-153. https://doi.org/10.1680/geot.1960.10.4.129.

Chakraborty, A. and Goswami, D. (2016), "State of the art: Three dimensional (3D) slope-stability analysis", *Int. J. Geotech. Eng*., **10**(5), 493-498. https://doi.org/10.1080/19386362.2016.1172807.

Chen, R.H. and Chameau, J.L. (1983), "Three-dimensional limit equilibrium analysis of slopes", *Géotechnique*, **33**(1), 31-40. https://doi.org/10.1680/geot.1983.33.1.31.

Chen, W.F., Giger, M.W. and Fang, H.Y. (1969), "On the limit analysis of stability of slopes", *Soils Found*., **9**(4), 23-32. https://doi.org/10.3208/sandf1960.9.4_23.

Chen, Z., Mi, H., Zhang, F. and Wang, X. (2003), "A simplified method for 3D slope stability analysis", *Can. Geotech. J*., **40**(3), 675-683. https://doi.org/10.1139/t03-002

Cheng, Y.M. and Yip, C.J. (2007), "Three-dimensional asymmetrical slope stability analysis extension of Bishop's, Janbu's, and Morgenstern-Price's techniques", *J. Geotech. Geoenviron. Eng*., **133**(12), 1544-1555. https://doi.org/10.1061/(ASCE)1090-0241(2007)133:12(1544).

Cousins, B.F. (1978), "Stability charts for simple earth slopes", *J. Geotech. Eng. Div*., **104**(2), 267-279.

Cousins, B.F. (1980), "Stability charts for simple earth slopes allowing for tension cracks", *Proceedings of the 3rd Australia-New Zealand Conference on Geomechanics,* Wellington, New Zealand, May.

Ganjian, N., Askari, F. and Farzaneh, O. (2010), "Influences of nonassociated flow rules on three-dimensional seismic stability of loaded slopes", *J. Cent. South Univ. Technol*., **17**(3), 603-611. https://doi.org/10.1007/s11771-010-0529-x

Gao, Y., Wu, D., Zhang, F., Lei, G.H., Qin, H. and Qiu, Y. (2016), Limit analysis of 3D rock slope stability with non-linear failure criterion", *Geomech. Eng*., **10**(1), 59-76. https://doi.org/10.12989/gae.2016.10.1.059

Gao, Y., Zhu, D., Zhang, F., Lei, G.H. and Qin, H. (2014), "Stability analysis of three-dimensional slopes under water drawdown conditions", *Can. Geotech. J*., **51**(11), 1355-1364. https://doi.org/10.1139/cgj-2013-0448.

Gao, Y.F., Zhang, F., Lei, G.H. and Li, D.Y. (2013), "An extended limit analysis of three-dimensional slope stability", *Géotechnique*, **63**(6), 518-524. https://doi.org/10.1680/geot.12.T.004.

Gens, A., Hutchinson, J.N. and Cavounidis, S. (1988), "Three-dimensional analysis of slides in cohesive soils", *Geotechnique*, **38**(1), 1-23. https://doi.org/10.1680/geot.1988.38.1.1.

Hovland, H.J. (1979), "Three-dimensional slope stability analysis method", *J. Geotech. Geoenviron. Eng*., **105(**5), 693-695.

Huang, C.C., Tsai, C.C. and Chen, Y.H. (2002), "Generalized method for three-dimensional slope stability analysis", *J. Geotech. Geoenviron. Eng*., **128**(10), 836-848. https://doi.org/10.1061/(ASCE)1090-0241(2002)128:10(836).

Hungr, O. (1987), "An extension of Bishop's simplified method of slope stability analysis to three dimensions", *Geotechnique*, **37**(1), 113-117. https://doi.org/10.1680/geot.1987.37.1.113.

Hungr, O., Salgado, F.M. and Byrne, P.M. (1989), "Evaluation of a three-dimensional method of slope stability analysis", *Can. Geotech. J*., **26**(4), 679-686. https://doi.org/10.1139/t89-079.

Janbu, N. (1954), "Stability analysis of slopes with dimensionless parameters", Division of Engineering and Applied Physics, Harvard University Soil Mechanics Series, Harvard University, Massachusetts, U.S.A.

Janbu, N. (1967), "Dimensionless parameters for homogeneous earth slopes", *J Soil Mech. Found. Div*., **93**(6), 367-374.

Janbu, N. (1968), "Slope stability computations", Soil Mechanics and Foundation Engineering Report, The Technical University of Norway, Norway.

Jeldes, I.A., Vence, N.E. and Drumm, E.C. (2015), "Approximate solution to the Sokolovskiĭ concave slope at limiting equilibrium", *Int. J. Geomech*., **15**(2), 04014049. https://doi.org/10.1061/(ASCE)GM.1943-5622.0000330

Kalatehjari, R. and Ali, N. (2013), "A review of three-dimensional slope stability analyses based on limit equilibrium method", *Electron. J. Geotech. Eng*., **18**, 119-134.

Leshchinsky, D. and Huang, C.C. (1992), "Generalized three-dimensional slope-stability analysis", *J. Geotech. Eng*., **118**(11), 1748-1764. https://doi.org/10.1061/(ASCE)0733-9410(1992)118:11(1748).

Leshchinsky, D., Baker, R. and Silver, M.L. (1985), "Three dimensional analysis of slope stability", *Int. J. Numer. Anal. Meth. Geomech*., **9**(3), 199-223. https://doi.org/10.1002/nag.1610090302.

Lim, K., Lyamin, A.V., Cassidy, M.J. and Li, A.J. (2016), "Three-dimensional slope stability charts for frictional fill materials placed on purely cohesive clay", *Int. J. Geomech*., **16**(2), 04015042. https://doi.org/10.1061/(ASCE)GM.1943-5622.0000526.

Lin, H.D., Wang, W.C. and Li, A.J. (2020), "Investigation of dilatancy angle effects on slope stability using the 3D finite element method strength reduction technique", *Comput. Geotech*., **118**, 103295. https://doi.org/10.1016/j.compgeo.2019.103295.

Liu, G., Zhuang, X. and Cui, Z. (2017), "Three-dimensional slope stability analysis using independent cover based numerical manifold and vector method", *Eng. Geol*., **225**, 83-95. https://doi.org/10.1016/j.enggeo.2017.02.022.

Michalowski, R.L. (2010), "Limit analysis and stability charts for 3D slope failures", *J. Geotech. Geoenviron. Eng*., **136**(4), 583-593. https://doi.org/10.1061/(ASCE)GT.1943-5606.0000251.

Michalowski, R.L. and Drescher, A. (2009), "Three-dimensional stability of slopes and excavations", *Géotechnique*, **59**(10), 839-850. https://doi.org/10.1680/geot.8.P.136.

Michalowski, R.L. and Tabetha, M. (2011), "Stability charts for 3D failures of steep slopes subjected to seismic excitation", *J. Geotech. Geoenviron. Eng*., **137**(2), 183-189. https://doi.org/10.1061/(ASCE)GT.1943-5606.0000412.

Morimasa, S. and Miura, K. (2008), "Three-dimensional slope stability analysis by means of limit equilibrium method", *Proceedings of the 10th International Symposium on Landslides and Engineered Slopes: From the Past to the Future*, Xi'an, China, June-July.

Nadukuru, S.S., Martel, T. and Michalowski, R.L. (2011), "3D analysis of steep slopes subjected to seismic excitation", *Proceedings of Geo-Frontiers 2011*, Dallas, Texas, U.S.A., March.

Pan, Q., Xu, J. and Dias, D. (2017), "Three-dimensional stability of a slope subjected to seepage forces", *Int. J. Geomech*., **17**(8), 04017035. https://doi.org/10.1061/(ASCE)GM.1943-5622.0000913

Pantelidis, L. and Griffiths, D.V. (2012), "Stability assessment of slopes using different factoring strategies", *J. Geotech. Geoenviron. Eng*., **138**(9), 1158-1160. https://doi.org/10.1061/(ASCE)GT.1943-5606.0000678.

Pantelidis, L. and Griffiths, D.V. (2013a), "Stability of earth slopes. Part I: Two-dimensional analysis in closed-form", *Int. J. Numer. Anal. Meth. Geomech*., **37**(13), 1969-1986. https://doi.org/10.1002/nag.2118.

Pantelidis, L. and Griffiths, D.V. (2013b), "Stability of earth slopes. Part II: three dimensional analysis in closed-form", *Int.*

J. Numer. Anal. Meth. Geomech., **37**(13), 1987-2004. https://doi.org/10.1002/nag.2116.

Pantelidis, L. and Griffiths, D.V. (2013c), "Integrating Eurocode 7 (load and resistance factor design) using nonconventional factoring strategies in slope stability analysis", *Can. Geotech. J.*, **51**(2), 208-216. https://doi.org/10.1139/cgj-2013-0239.

Pantelidis, L. and Psaltou, E. (2012), "Stability tables for homogeneous earth slopes with benches", *Int. J. Geotech. Eng.*, **6**(3), 381-394. https://doi.org/10.3328/IJGE.2012.06.03.381-394.

Spencer, E. (1967), "A method of analysis of the stability of embankments assuming parallel inter-slice forces", *Géotechnique*, **17**(1), 11-26. https://doi.org/10.1680/geot.1967.17.1.11.

Sun, C., Chai, J., Ma, B., Luo, T., Gao, Y. and Qiu, H. (2019), "Stability charts for pseudostatic stability analysis of 3D homogeneous soil slopes using strength reduction finite element method", *Adv. Civ. Eng.*, 1-18. https://doi.org/10.1155/2019/6025698.

Sun, C., Chai, J., Xu, Z. and Qin, Y. (2017), "3D stability charts for convex and concave slopes in plan view with homogeneous soil based on the strength-reduction method", *Int. J. Geomech.*, **17**(5), 06016034. https://doi.org/10.1061/(ASCE)GM.1943-5622.0000809.

Sun, G., Zheng, H. and Jiang, W. (2012), "A global procedure for evaluating stability of three-dimensional slopes", *Nat. Hazards*, **61**(3), 1083-1098. https://doi.org/10.1007/s11069-011-9963-9.

Taylor, D. (1948), *Fundamentals of soil mechanics*, Chapman and Hall, Limited, New York, U.S.A.

Ugai, K. (1988), "Three-dimensional slope stability analysis by slice methods", *Proceedings of the 6th International Conference on Numerical Methods in Geomechanics*, Innsbruck, Austria, April.

US Army Corps of Engineers (1990), "Engineering and design - Settlement analysis", EM 1110-1-1904, US Army Corps of Engineers.

Wang, L., Hu, W., Sun, D. and Li, L. (2019) "3D stability of unsaturated soil slopes with tension cracks under steady infiltrations", *Int. J. Numer. Anal. Meth. Geomech.*, **43**(6), 1184-1206. https://doi.org/10.1002/nag.2889

Xing, Z. (1988), "Three-dimensional stability analysis of concave slopes in plan view", *J. Geotech. Eng.*, **114**(6), 658-671. https://doi.org/10.1061/(ASCE)0733-9410(1988)114:6(658).

Xu, J., Li, Y. and Yang, X. (2018), "Stability charts and reinforcement with piles in 3D nonhomogeneous and anisotropic soil slope", *Geomech. Eng.*, **14**(1), 71-81. https://doi.org/10.12989/gae.2018.14.1.071.

Xu, J.S. and Yang, X.L. (2018) "Three-dimensional stability analysis of slope in unsaturated soils considering strength nonlinearity under water drawdown", *Eng. Geol.*, **237**, 102-115. https://doi.org/10.1016/j.enggeo.2018.02.010.

Yamagami, T. and Jiang, J.C. (1997), "A search for the critical slip surface in three-dimensional slope stability analysis", *Soils Found.*, **37**(3), 1-16. https://doi.org/10.3208/sandf.37.3_1.

Yamaguchi, K., Takeuchi, N. and Hamasaki, E. (2018), "Three-dimensional simplified slope stability analysis by hybrid-type penalty method", *Geomech. Eng.*, **15**(4), 947-955. https://doi.org/10.12989/gae.2018.15.4.947.

Yang, X.L. (2017), "Effect of pore-water pressure on 3D stability of rock slope", *Int. J. Geomech.*, **17**(9), 06017015. https://doi.org/10.1061/(ASCE)GM.1943-5622.0000969.

Yang, X.L. and Xu, J. (2017), "Three-dimensional stability of two-stage slope in inhomogeneous soils", *Int. J. Geomech.*, **17**(7), 06016045. https://doi.org/10.1061/(ASCE)GM.1943-5622.0000867.

Zhang, T., Cai, Q., Han, L., Shu, J. and Zhou, W. (2017), "3D stability analysis method of concave slope based on the Bishop method", *Int. J. Min. Sci. Technol.*, **27**(2), 365-370. https://doi.org/10.1016/j.ijmst.2017.01.020.

Zhang, Y., Chen, G., Wang, B. and Li, L. (2013a), "An analytical method to evaluate the effect of a turning corner on 3D slope stability", *Comput. Geotech.*, **53**, 40-45. https://doi.org/10.1016/j.compgeo.2013.05.002.

Zhang, Y., Chen, G., Zheng, L., Li, Y. and Zhuang, X. (2013b), "Effects of geometries on three-dimensional slope stability", *Can. Geotech. J.*, **50**(3), 233-249. https://doi.org/10.1139/cgj-2012-0279.

Zhou, X.P. and Cheng, H. (2013), "Analysis of stability of three-dimensional slopes using the rigorous limit equilibrium method", *Eng. Geol.*, **160**, 21-33. https://doi.org/10.1016/j.enggeo.2013.03.027.

CC